Clustering of Zirconium Atoms in Zr_5Te_6: A Novel NiAs-Type-Related Telluride with Ordered Vacancies

Gissur Örlygsson and Bernd Harbrecht*[a]

Abstract: Zr_5Te_6 has been synthesized and its structure determined by means of single crystal X-ray diffraction to be trigonal, $P\bar{3}m1$, $Z = 3$, Pearson symbol $hP33$, $a = 1172.8(2)$ pm, $c = 707.0(1)$ pm. Zr_5Te_6 adopts a metal-deficient, vacancy-ordered $3a \times 3a \times 1c$ superstructure of the NiAs type structure. In the Zr atom layers, alternately one and two out of nine Zr atoms are missing. The less densely populated layers (7/9) consist of star-shaped Zr_7 clusters with intracluster contacts of 351.1 pm; the shortest Zr–Zr intercluster distance is 470.5 pm. In the more densely populated Zr atom layers (8/9), three quarters of the Zr atoms are arranged to pairs (326.4 pm). The distinctive distribution of the vacancies affords a topologically uniform fivefold Zr coordination (283.5–302.6 pm) for all three crystallographically inequivalent Te atoms. They are shifted towards the vacancies in the Zr atom layers. The associated corrugation of the Te atom layers is characterized by an amplitude of 28 pm. The Te–Te contacts are ≥ 368.1 pm. According to extended Hückel calculations, the defects in the Zr atom layers lead to a reduction in overall Zr–Te bonding interactions relative to ZrTe (NiAs). However, through the clustering the total attractive intralayer Zr–Zr interactions increase considerably, thus providing decisive stabilization of the structure. As revealed by thermal analyses, Zr_5Te_6 undergoes a reversible phase transition at 1513 ± 5 K. On the Zr-rich side, Zr_5Te_6 coexists with ZrTe (WC), and, above 1438 ± 5 K with the hitherto unknown ZrTe (MnP). Zr_5Te_6 exhibits temperature independent paramagnetic properties ($\chi_{mol} = 0.7 \times 10^{-3}$ cm^3 mol^{-1}) that are typical for a metallic conductor. An abrupt increase in the magnitude of the diamagnetic susceptibility below 2.2 K in a weak magnetic field indicates a superconducting transition.

Keywords: cluster compounds · electronic structure · magnetic properties · tellurium · zirconium

Introduction

Metal-rich tellurides of the valence-electron-poor transition metals uncovered during the last decade, for example, Sc_9Te_2,[1] Hf_3Te_2[2] and dd-$Ta_{1.6}Te$,[3] adopt structures with varying, and often intriguing characteristic features. Tellurium-rich compounds of those metals also provide unforeseen examples of structural diversity. In this vein, the homologous sesquitellurides Nb_2Te_3[4] and Ta_2Te_3[5] have different structure types; this is in contrast to the common textbook notion of a similar chemical behaviour of 4d and 5d elements. Supplementing, and partly rectifying earlier findings,[6] research in the Zr–Te system also has brought to light new binary compounds in recent years. A survey of the literature shows that in the tellurium-rich part of the system $ZrTe_5$,[7] $ZrTe_3$,[8] $ZrTe_2$[9, 10] and $Zr_{1.3}Te_2$[11] have been characterized. At equiatomic composition, ZrTe (WC)[12, 13] and ZrTe (MnP)[14] exist. In the metal-rich part, Zr_5Te_4,[12, 15, 16] Zr_3Te[16, 17] and Zr_2Te[18] have been reported. In addition to an earlier partial phase diagram,[19] a tentative phase diagram of the system was published lately,[20] which contained some valuable hints for preparative work.

We report here the synthesis of a novel binary zirconium telluride Zr_5Te_6,[21] and its characterization by using single-crystal and powder X-ray diffractometry, differential scanning calorimetry (DSC) measurements, energy-dispersive X-ray (EDX) analysis, magnetic susceptibility measurements, and extended Hückel calculations. Zr_5Te_6 adopts a NiAs-type-related structure with ordered vacancies. Examples of phases with ordered vacancies are found in the Ti–S[22] and Cr–S,[23] in which Cr_5S_6 was observed, systems. As opposed to Zr_5Te_6, the metal vacancies in those phases are confined to every second layer of metal atoms. The intralayer clustering of Zr atoms in Zr_5Te_6 is reminiscent of that resulting from charge-density wave transitions in some Group 5 transition metal dichalcogenides.[24, 25] Parallels can be drawn to d-electron-dependent clustering patterns in related transition metal compounds.[26] Bearing in mind the inevitable reduction in the frequency of hetero- and homonuclear bonding interactions that result from the defects in the Zr atom layers in Zr_5Te_6 relative to hypothetical stoichiometric ZrTe (NiAs type), it is instructive to scrutinize the bonding situation in Zr_5Te_6.

[a] Prof. Dr. B. Harbrecht, Dipl.-Chem. G. Örlygsson
Department of Chemistry and Materials Science Centre
Philipps University, Hans-Meerwein-Str. 35032 Marburg (Germany)
Fax: (+49) 6421 2828917
E-mail: harbrecht@chemie.uni-marburg.de

0947-6539/00/0622-4170 $ 17.50+.50/0

Results and Discussion

Phase relations: Zr_5Te_6 is accessible from the melt. Arc-melted samples of equiatomic composition yielded a mixture consisting of Zr_5Te_6 and Zr_5Te_4. In addition, diffuse reflections of ZrTe (MnP)[14] were observed; this suggests an emergence of that phase during the cooling process. Preparative experiments reveal that Zr_5Te_6 has an extended stability region down to at least 1070 K. According to differential scanning calorimetry (DSC) experiments, in combination with phase analysis from X-ray powder diffraction, Zr_5Te_6 undergoes a reversible phase transition at 1513 ± 5 K. In the uppermost temperature region, Zr_5Te_6 coexists with Zr_5Te_4 as a neighbouring phase to the metal-rich side. DSC measurements show a first order, reconstructive phase transition from ZrTe (WC) to ZrTe (MnP) at 1438 ± 5 K; ZrTe (MnP) is stable up to at least 1770 K. The phase transition is reversible, although the reverse reaction is kinetically inhibited at room temperature. Thus, ZrTe (MnP) represents the next metal-rich phase to Zr_5Te_6 down to 1438 ± 5 K. Below 1438 ± 5 K this then becomes ZrTe (WC). The neighbouring phases on the tellurium-rich side of Zr_5Te_6 have still to be explored.

Abstract in German: *Das niedervalente Zirconiumtellurid Zr_5Te_6 wurde hergestellt. Einer Röntgenstrukturanalyse von einem meroedrisch verzwillingten Kristall zufolge kristallisiert Zr_5Te_6 trigonal in der Raumgruppe $P\bar{3}m1$, Pearson Symbol hP33, $a = 1172.8(2)$ pm, $c = 707.0(1)$ pm. Die Struktur entspricht einer metalldefizienten $3a \times 3a \times 1c$-Überstruktur des NiAs-Typs mit geordneten Leerstellen. In den Zr-Atomschichten fehlen abwechselnd eins und zwei von neun Zr-Atomen. Die weniger dicht belegten Schichten (7/9) enthalten sternförmige Zr_7-Cluster mit Intraclusterkontakten von 351.1 pm. Die kürzesten Interclusterabstände betragen 470.5 pm. In den dichter belegten Schichten sind dreiviertel der Zr-Atome im Abstand von 326.4 pm zu Paaren angeordnet. Die spezifische Verteilung der Leerstellen geht mit einer topologisch einheitlichen, fünffachen Koordination der drei kristallographisch ungleichen Te-Atome einher. Die Veschiebung der Te-Atome in Richtung der Lücken führt zu einer Wellung der Te-Atomschichten mit einer Amplitude von 28 pm und Te – Te-Kontakten ≥ 368.1 pm. Extended-Hückel-Rechnungen nach bedingen die Defekte in den Zr-Atomschichten verglichen mit ZrTe (NiAs) eine Verminderung heteronuklearer Bindungen, wohingegen die Zr – Zr-Wechselwirkungen innerhalb der Schicht trotz der Unterbesetzung infolge der Clusterung deutlich verstärkt sind, wodurch die Struktur entscheidend stabilisiert wird. Zr_5Te_6 durchläuft bei 1513 ± 5 K eine reversible Phasenumwandlung. Auf der Zr-reichen Seite koexistiert es mit ZrTe (WC) und oberhalb 1438 ± 5 K mit ZrTe (MnP). Zr_5Te_6 zeigt einen für Metalle typischen temperaturunabhängigen Paramagnetismus ($\chi_{mol} = 0.7 \times 10^{-3}$ cm^3 mol^{-1}). Ein steiler Abfall der diamagnetischen Suszeptibilität unterhalb 2.2 K im schwachen Magnetfeld verweist auf einen Übergang in den supraleitenden Zustand.*

Structural features: The crystal structure of Zr_5Te_6 represents a new, metal-deficient, vacancy-ordered $3a \times 3a \times 1c$ superstructure of the NiAs type. The NiAs-type structure is based on a hexagonal close packed arrangement of the non-metal atoms (A, B) according to the sequence AcBcA. Hence, it consists of condensed trigonal prismatic Zr_6 clusters, every second of which is stabilized by an interstitial Te atom, whereas the Zr atoms are octahedrally coordinated with Te atoms. Zr_5Te_6 is composed of seven symmetrically inequivalent atoms, Te1 – Te3 and Zr1 – Zr4. In the two Zr-atom layers, alternately one and two out of nine Zr atoms of a fully occupied layer are missing (Figure 1a and b). The specific distribution of the vacancies leads to a uniform fivefold coordination of the three distinct Te atoms, which corresponds to a distorted trigonal prism with one Zr atom absent (Figure 2). The Zr atoms are coordinated by Te in a distorted octahedron ($d_{Zr-Te} = 283.5 - 302.6$ pm); Figure 1c. The Zr atoms in the less densely populated layer (7/9) show a distinct clustering: six Zr atoms surround a central one with a distance of 351.1 pm between the atoms, while the distance between the Zr_7 clusters is 470.5 pm (Figure 1b). The shortest distance between Zr atoms in neighbouring Zr atom layers is 360.8 pm. The shortest Zr–Zr distance (326.4 pm) is found in the more densely populated Zr atom layer (8/9), in which pairing is observed. In the Te atom layers all positions are occupied (9/9), with the Te atoms shifted towards the vacancies in the Zr atom layers. This leads to a considerable corrugation of the Te atom layers, with an amplitude of ~ 28 pm. The Te – Te contacts (≥ 368.1 pm) indicate Te – Te van der Waals interactions.

Structural comparison and clustering patterns in related d^n electron systems: From layered-type chalcogenides, various clustering patterns are known, depending on the number of d electrons available for homonuclear metal – metal bonding.[26] In d^1 systems, the formation of discrete clusters is observed, for example, seven and thirteen atom clusters in the low temperature superstructures of $2H$-$TaSe_2$ ($3a \times 3a \times 1c$, < 90 K) and $1T$-$TaSe_2$ (< 473 K), respectively.[24] In the former phase, seven of nine atoms in a layer participate in the cluster formation. It can be anticipated, that the two atoms that do not participate are less reduced (d^{1-x}) than the seven atoms in the clusters (d^{1+y}). Upon moving to a d^2 system, for example, β-$MoTe_2$, the metal atoms link up to form zigzag chains.[27] In these three phases, no significant chalcogen to metal ($p \rightarrow d$) electron transfer is predicted.[28, 29] This situation changes in the low-temperature superstructure of VTe_2 (< 482 K),[30] in which internal redox competition leads to a transfer of electrons from Te to V, and a formal d electron count in the range from 1.25 to 2 instead of 1.[31] Accompanied with the depopulation of the Te p-block orbitals is the formation of weak Te–Te bonds in the structure. The associated gain in V d-electron density leads to the formation of double zigzag chains of metal atoms, a "compromise"[31] between the formation of discrete clusters and single zigzag chains. This same type of clustering is also found in $NbTe_2$ and $TaTe_2$.[32]

Turning again to the zirconium tellurides, $ZrTe_2$[9] represents an undistorted, ideal CdI_2 type structure, with regular

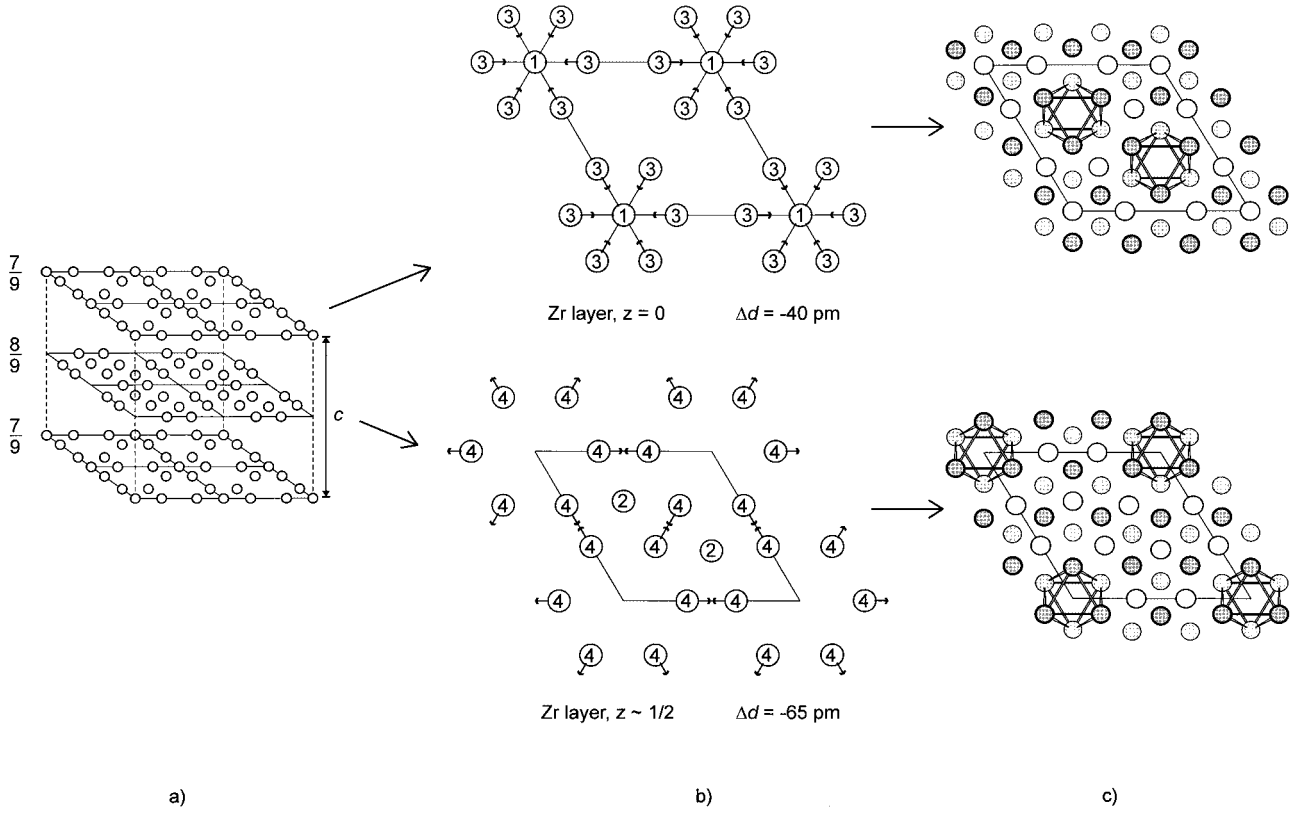

Figure 1. Details of the crystal structure of Zr_5Te_6. a) Zr partial structure; four unit cells are shown, indicated by lines. Note that for the sake of clarity the *c* axis is expanded. b) Vacancy ordering in the Zr atom layers. The displacement direction and magnitude (Δd) of the atoms with respect to the NiAs-type atom coordinates (model **b**; see Experimental Section) are indicated. Projection along [001]. c) Te coordination of the Zr atoms. The distorted octahedra around the vacancies are emphasized. Shaded circles represent Te atoms, open circles Zr atoms. Thin-bordered circles are located below and thick-bordered cicles above the Zr atom plane. Projection along [001].

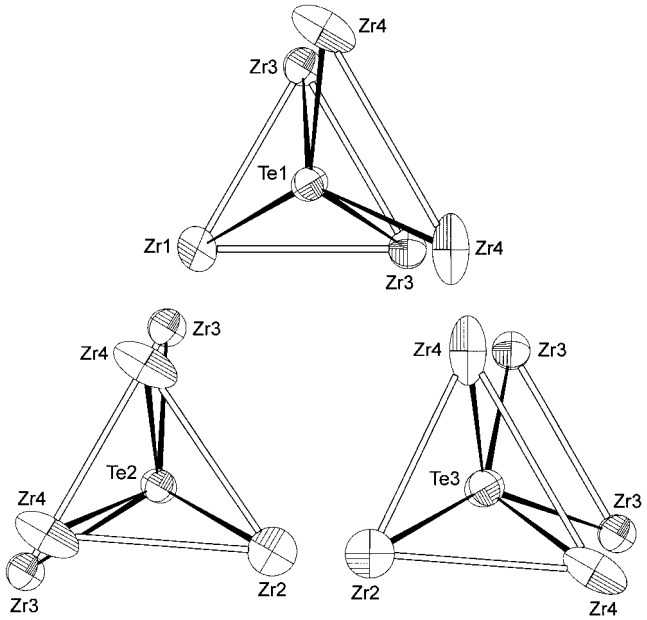

Figure 2. The distorted trigonally prismatic coordination-spheres of the Te atoms in Zr_5Te_6; one Zr atom is always absent. Anisotropic displacements (99.9% probability) are shown.

hexagonal layers of Zr atoms, typical for d^0 systems. In the newly discovered ZrTe (MnP),[14] in which the formal oxidation state of Zr is +2 (d^2), the metal atoms form zigzag chains. For Zr_5Te_6, an average d-electron count of 1.6 can be calculated, again assuming fully reduced Te (−2). Treating the two Zr atom layers separately yields $d^{1.75}$ (Zr_8Te_9) and $d^{1.43}$ (Zr_7Te_9). In the 7/9 layer, seven-atom clusters are formed. Based on the number of d electrons available for homonuclear metal–metal bonding, and by employing the results from the dichalcogenides, one could also have expected double zigzag chains to form. This, of course, is impossible due to the vacancies present. Instead, discrete clusters are formed. An important feature of this type of clustering compared with other conceivable patterns, especially considering the high synthesis temperatures employed, is that trigonal symmetry is retained. The clustering in the 8/9 layer, with distinctive pair formation, shows certain characteristic attributes of the previously discussed zigzag chains. Interestingly, the shortest Zr–Zr distance in Zr_5Te_6 (326.4 pm), which is found in this strongly bonded pair, is in close match with that found in the zigzag chain of ZrTe (MnP) (326.0 pm). Results of extended Hückel calculations give no reasons to assume a considerable $p \rightarrow d$ electron transfer from Te to Zr in Zr_5Te_6.

The recently reported zirconium telluride $Zr_{1.30}Te_2$[11] shows, in contrast to Zr_5Te_6, a random occupation of one third of the metal atom sites in every second layer. The other metal atom layer is completely filled. No clustering of Zr atoms is observed. To our knowledge, clustering or vacancy ordering similar to that found in Zr_5Te_6, in a comparable composition range (50–60 atomic% chalcogen or pnicogen) does not exist

  0947-6539/00/0622-4172 $ 17.50+.50/0

in related binary systems. For and around the composition $Ti_{0.66}S$,[22] as well as in V_3S_4[33] and V_3Se_4,[34] vacancy ordering in every second metal atom layer is observed. This also holds for several chromium sulfides in the region $CrS-Cr_{0.66}S$.[23] In Cr_5S_6, which crystallizes in a $3^{1/2}a \times 3^{1/2}a \times 2c$ superstructure of the NiAs type, one out of three metal atom sites in every second metal atom layer is vacant.

Electronic structure—comparison with ZrTe (NiAs type) and two hypothetical Zr_5Te_6 models: Band structure calculations on Zr_5Te_6, two hypothetical Zr_5Te_6 models **a** and **b**, and on a hypothetical stoichiometric ZrTe (NiAs type) were carried out by using the extended Hückel method. For details on models **a** and **b** refer to the Experimental Section.

According to the total density of states (DOS) diagrams for Zr_5Te_6 and a hypothetical Zr_5Te_6 (model **a**) derived from NiAs-type ZrTe coordinates and lattice shown in Figure 3, the

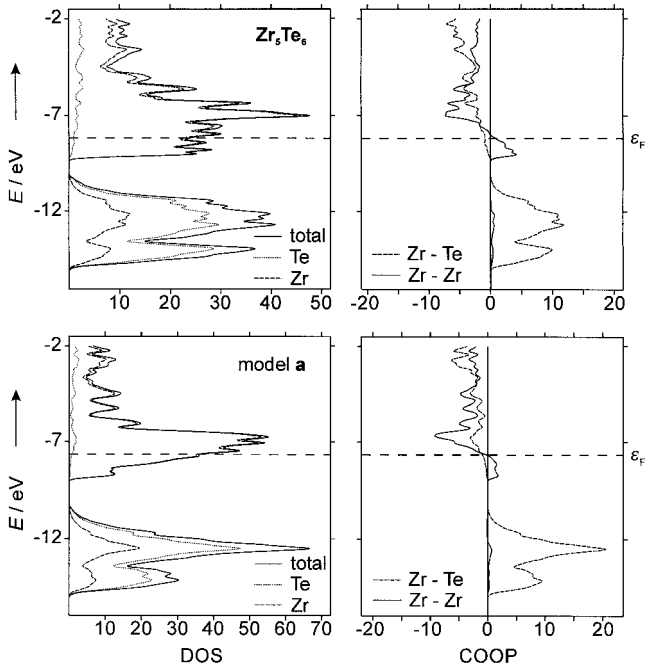

Figure 3. Densities of states (DOS), and crystal orbital overlap population (COOP) curves for Zr_5Te_6, and a hypothetical Zr_5Te_6 with NiAs-type ZrTe coordinates and lattice ($3a \times 3a \times 1c$), model **a**. COOP curves for Zr–Te contacts up to 303 pm (283 pm) and Zr–Zr contacts up to 423 pm (396 pm) for Zr_5Te_6 (model **a**) are shown. Levels up to the Fermi energy (broken horizontal line) are filled; levels to the right of the vertical line are bonding, to the left are antibonding. The Fermi energy for Zr_5Te_6 lies at -8.2 eV, for model **a** at -7.7 eV.

Fermi level (ε_F) lies in both cases in regions that are dominated by Zr d-orbital contributions. The Te p-orbital contributions extend in both cases downwards from about 2.5 eV below ε_F. The better tuning of the Zr–Zr bonds in real Zr_5Te_6 compared with model **a** is clearly reflected in the DOS and crystal orbital overlap population (COOP) curves shown in Figure 3; the distortions associated with the cluster formation give rise to a shift of Zr d states down to lower energies, concomitantly making more states available for homonuclear bonding interactions. The hypothetical rearrangement from model **a** to the real Zr_5Te_6 structure is further accompanied by a lowering of the Fermi level from -7.7 eV to -8.2 eV, indicative of the energetically favourable process.

Based on ZrTe NiAs-type-derived metal atom positions in a Zr_5Te_6-type identical lattice (model **b**), the metal atom displacements found in the Zr_7 clusters and the Zr_2 pairs in Zr_5Te_6 amount to 40 and 65 pm, respectively (Figure 1b). For comparison, similar clustering of seven metal atoms in 2*H*-TaS_2, but without vacancies present, results in around ten times smaller atomic displacements of approximately 5 pm. The average Mulliken overlap population per intralayer metal–metal bond increases slightly upon the clustering,[29] providing a driving force for the process.

The Mulliken overlap population (MOP)[35] for a given pair of atoms in a specified phase, real or hypothetical, can be seen as an expression for the strength of bonding interactions. Thus, the MOP can be employed in a qualitative assessment and comparison of the bonding situation in different phases. Judging from the summation of the MOPs, the Zr–Te interactions in ZrTe (NiAs) and Zr_5Te_6 represent the bulk of the bonding interactions in those phases (Table 1). In total,

Table 1. Mulliken overlap populations (MOP). Comparison of Zr_5Te_6 with ZrTe (NiAs-Type) and two hypothetical Zr_5Te_6 models **a** and **b** (see Experimental Section for details).

	ZrTe	Zr_5Te_6 (**a**)	Zr_5Te_6 (**b**)	Zr_5Te_6
	NiAs type coordinates			
Interaction		NiAs-type lattice	Zr_5Te_6 lattice	
Zr–Zr intralayer	2.25	1.24	1.87	3.39
Zr–Zr interlayer	1.95	1.46	0.89	0.88
Zr–Zr total	4.20	2.70	2.76	4.27
Zr–Te total	41.0	39.1	38.5	35.8

the Zr–Zr interactions in both phases are very similar. Surprisingly, in spite of the vacancies in the Zr atom layers in Zr_5Te_6, the sum of the Zr–Zr overlap populations in the (001) plane is considerably larger than in ZrTe (NiAs) (3.39 vs. 2.25). The decrease in interlayer Zr–Zr interactions as a result of the vacancies, on the other hand, leads to much smaller total interlayer Zr–Zr overlap populations in Zr_5Te_6 than in ZrTe (NiAs) (0.88 vs. 1.95). This is also reflected in the larger *c* lattice parameter of Zr_5Te_6. Following the development of the summation of overlap populations from ZrTe (NiAs) over the two hypothetical models **a** and **b** to Zr_5Te_6 shows a continuous and expected decrease in total Zr–Te interactions and interlayer Zr–Zr interactions (Table 1). Tracing this development for the intralayer Zr–Zr interactions gives an idea of the importance of the shifts of the Zr atoms away from the NiAs-type positions to the coordinates of the Zr_5Te_6 structure for the optimization of the Zr–Zr interactions in the layers. Thus, removal of the Zr atoms from the NiAs-type lattice results in a reduction of bonding interactions ($2.25 \rightarrow 1.24$); this is partly compensated for ($1.24 \rightarrow 1.87$) on adoption of the dimensions of the Zr_5Te_6 lattice. The clustering of the Zr atoms finally brings a drastic increase in bonding interactions in the (001) plane ($1.87 \rightarrow 3.39$).

Magnetic susceptibility: The temperature dependence of the magnetic susceptibility is shown in Figure 4a. The essentially temperature-independent paramagnetic susceptibility observed ($\chi_{mol} = 0.7 \times 10^{-3}$ cm^3 mol^{-1}) is typical of materials with metallic transport properties and unpaired conduction electrons. A field-independent susceptibility was obtained at 5 K.

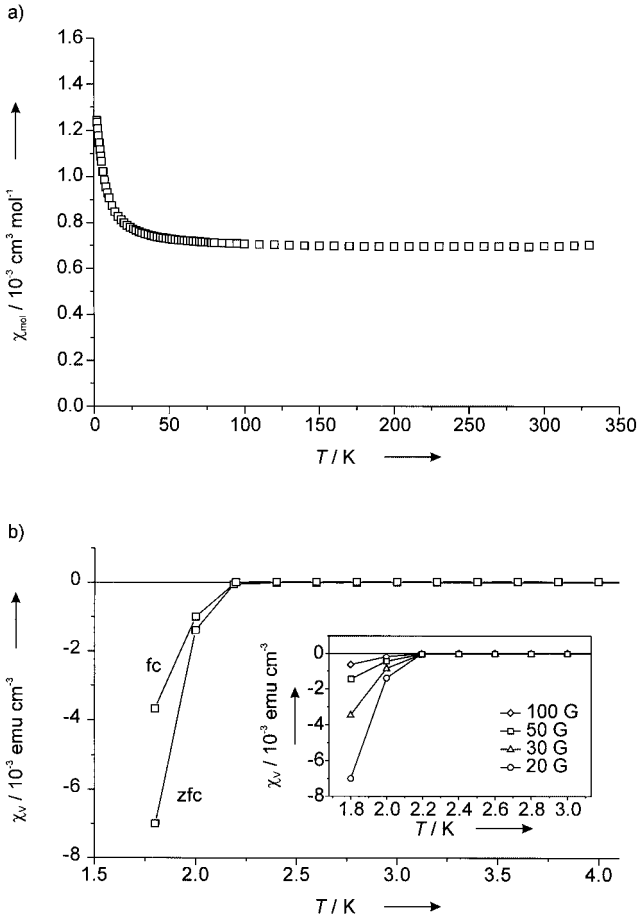

Figure 4. Magnetic properties of Zr_5Te_6 (powder sample). a) Temperature dependence of the molar magnetic susceptibility measured at a field of 30 kG. b) Evidence for a superconducting transition in Zr_5Te_6. Diamagnetic shielding is observed for zero-field cooling (zfc) in an external field of 20 G; the Meissner effect is observed for field cooling (fc). Inset: field-dependence of the superconducting transition (zfc data) at 20, 30, 50, and 100 G external magnetic field.

The abrupt increase in the magnitude of the diamagnetic susceptibility of Zr_5Te_6 below 2.2 K (onset) in a weak magnetic field points to a transition into a superconducting state. Figure 4b shows the observed diamagnetic shielding for zero-field cooling (zfc), the Meissner effect for field cooling (fc) and the dependence of the transition on field strength. Due to instrumental limitations, the data collection had to be interrupted while readings were moving rapidly to more negative magnetization values (fc case). Estimating the lower limit of the superconducting volume fraction at 1.8 K from the volume susceptibility (χ_V), after cooling in an external magnetic field of 20 G, yields 4.6% of the theoretical value ($-1/4\pi$). According to a hysteresis loop cycled over $-150\ \mathrm{G} \le B_{app} \le 150\ \mathrm{G}$ at 1.8 K, B_{c1} can be estimated to be 10 ± 3 G. Magnetic susceptibility measurements on Zr_5Te_4 and the neighbouring phase ZrTe (MnP)[14] did not indicate superconductivity in those phases above 1.8 K. A superconducting transition occurs in Zr at 0.61 K.[36]

Conclusion

The zirconium telluride Zr_5Te_6 is identified as the phase that coexists with ZrTe (WC), and above 1438 ± 5 K up to at least 1770 K with ZrTe (MnP). Starting from $ZrTe_2$ and Zr, Zr_5Te_6 forms readily at 1470 K. Zr_5Te_6 undergoes a reversible phase transition at 1513 ± 5 K. The susceptibilities became strongly diamagnetic in weak external fields below 2.2 K, an indication of a transition into a superconducting state.

At ambient temperature, Zr_5Te_6 adopts a NiAs-type $3a \times 3a \times 1c$ superstructure. It exhibits a unique pattern of vacancies in the metal atom layers, together with a distinctive clustering of Zr atoms. Consecutive layers, with one and two out of nine metal atom positions being empty, comprise alternately Zr_2 pairs and star-shaped Zr_7 clusters, respectively. The specific vacancy ordering underlying the clustering of Zr atoms ensures the three crystallographically inequivalent Te atoms a similar fivefold Zr coordination.

The ordering phenomena are correlated with clustering that is dependent on the the d-electron count of Group 5 and 6 transition metal chalcogenides. The enhancement in Zr–Zr bond energy brought about by the clustering overcompensates the configurational entropy term in the free energy for an alternative disordered defect NiAs-type structure, even at temperatures as high as 1513 K. In fact, comparative extended Hückel calculations reveal a decisive contribution of the cluster energy to the stability of Zr_5Te_6.

A series of complex phases with modulated structures, following Zr_5Te_6 in the Te-rich domain, await to be unravelled.

Experimental Section

Preparation: Due to their air-sensitivity, the tellurides were handled and stored under argon. The starting material $ZrTe_2$ was prepared from the elements (Te: 99.999%, Fluka; Zr: 99.8%, ChemPur; $n_{Zr}:n_{Te} = 1:2$) in previously out-gassed, sealed quartz glass tubes (1150 K, 1 d). Single crystals of Zr_5Te_6 were obtained through the reduction of $ZrTe_2$ with Zr (1570 K, 3 d, I_2) in a sealed, argon-filled tantalum tube, which in turn was contained in an evacuated corundum tube ($P < 10^{-3}$ Pa). The temperature of the reaction mixture was uniformly raised over 12 h from room temperature to 1570 K, and lowered again over 9 h to room temperature. By means of energy-dispersive X-ray (EDX) spectroscopic analysis (CamScan CS4DV, EDX system, Noran Instruments, 30 kV, Zr-L, Te-L, Ta-L; detection limit: Be) no other elements than Zr and Te were found. EDX analysis of single crystals yielded $x_{Te} = 0.547(10)$.

DSC investigations: Differential scanning calorimetry (DSC) investigations were performed with help of a SETARAM Setsys 16/18 with PtRh 6%/PtRh 30% thermocouples. The samples (20–100 mg) were pressed into pellets (∅ 3.5 mm, 6.5 kN) and put in a molybdenum crucible, which subsequently was sealed under an argon atmosphere. The sample crucible, together with an empty reference crucible, was placed on the DSC transducer. The furnace compartment was evacuated ($P < 1$ Pa) and flooded with purified argon gas. This procedure was repeated three times before a measurement was conducted under a stream of purified argon. The heating rate used was 10 K min^{-1}; cooling rates were 10–40 K min^{-1}.

0947-6539/00/0622-4174 $ 17.50+.50/0 *Chem. Eur. J.* **2000**, *6*, No. 22

No significant weight changes of the molybdenum crucibles were detected. Reactions between molybdenum and the specimens were not observed.

Powder X-ray diffraction: Guinier X-ray powder diffraction was used as a characterization method for phase identification. Guinier photographs were obtained with a Huber Guinier System 600 with $Cu_{K\alpha_1}$ radiation. Silicon[37] was added to the samples as an internal standard. Lattice parameters were determined from Guinier diffraction data by least-squares refinement by using the local program DIFFRAKT.[38] X-ray powder diffractograms were recorded in transmission at ambient temperature on a Philips X'Pert MPD diffractometer with θ:θ geometry, equipped with a diffracted-beam curved graphite monochromator and $Mo_{K\alpha}$ radiation. Intensities were detected by means of a position-sensitive detector. The samples were held in a sealed glass capillary under an Ar atmosphere. An X-ray powder diffractogram and a Rietveld profile fit for Zr_5Te_6 are shown in Figure 5.

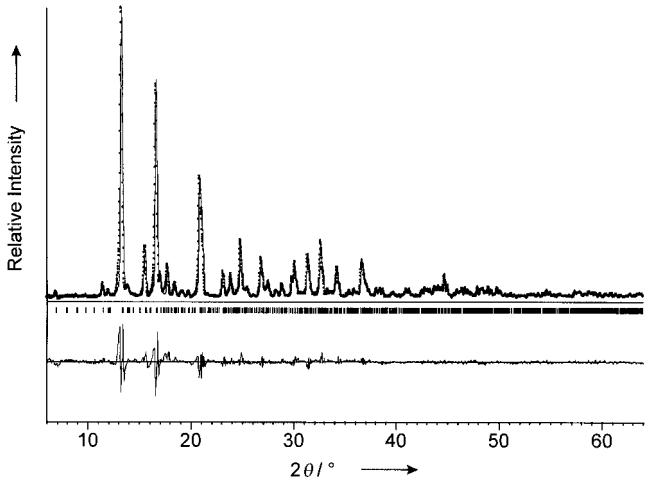

Figure 5. X-ray powder diffractogram ($Mo_{K\alpha}$) and a Rietveld profile fit of Zr_5Te_6 (top). Measured (dots) and calculated (line) intensities with a difference plot (bottom, 50 % expanded). In the middle the positions of the Bragg angles of Zr_5Te_6 are shown.

Single-crystal X-ray diffraction: The selected crystals were mounted in argon-filled glass capillaries. Relevant data for the single-crystal X-ray structure investigation of Zr_5Te_6 are given in Table 2. Positional parameters and isotropic, equivalent temperature factors are given in Table 3. Anisotropic temperature factors are given in Table 4. Selected interatomic distances are found in Table 5. On all crystals tested, twinning by merohedry was observed, with the twin plane (001). The structure could be solved without considering the twinning, but refinement of the structure parameters without applying the twin law led to poor residual values [$R(F_o) = 0.1508$; $R_w(F_o^2) = 0.2894$] and displacement parameters. On applying the twin law the residual values dropped to $R(F_o) = 0.0252$ and $R_w(F_o^2) = 0.0438$ and the displacement parameters improved drastically. A numerical absorption correction resulted in a minor improvement of the final residual factors to $R(F_o) = 0.0238$ and $R_w(F_o^2) = 0.0409$, as shown in Table 2. The lattice parameters determined for the single crystal on the basis of the positions of 5000 reflections, and those from Guinier powder diffraction data (65 reflections, $a = 1172.08(9)$, $c = 706.65(4)$ pm) are in good agreement. No signs of a partial occupation of the atomic sites were found. We note, that the orthorhombic lattice parameters of a phase reported at 52 atomic % Te[20] (Zr_5Te_6: 54.5 atomic % Te) can be transformed to the present hexagonal lattice parameters and agree within less than 1 pm in each case: $a_o = 706.35(6)$ pm $= c_h$; $b_o/3^{1/2} = 1172.3(1)$ pm $= a_h$; $c_o \times 3 = 1172.9(1)$ pm $= a_h$.

Further details on the crystal structure investigation may be obtained from the Fachinformationszentrum Karlsruhe, D-76344 Eggenstein-Leopoldshafen, Germany (fax: (+49) 7247-808-666; e-mail: crysdata@fiz-karlsruhe.de), on quoting the depository number CSD-411202.

Magnetic susceptibility measurements: Magnetic susceptibility measurements were carried out with the aid of a Quantum Design MPMS SQUID

Table 2. Selected crystallographic data for Zr_5Te_6.

formula	Zr_5Te_6
M_w [g mol^{-1}]	1221.72
space group; Z	trigonal, $P\bar{3}m1$ (No. 164); 3
a [pm]	1172.8(2)
c [pm]	707.0(1)
V [10^6 pm^3]	842.1(2)
ρ_{calcd} [g cm^{-3}]	7.227
μ [mm^{-1}]	19.70
data collection	
crystal	silver lustre, hexagonal plate
crystal size [mm^3]	$0.055 \times 0.065 \times 0.080$
diffractometer	IPDS (STOE & Cie)
T [K]	293
λ $Mo_{K\alpha}$ [pm]	71.073
monochromator	graphite
distance crystal-IP / mm	40
ϕ, $\phi_{incr.}$ [°]	0–300, 1.0
$2\theta_{max}$ [°]	65.7
index range	$-17 \le h \le +17$, $-17 \le k \le +17$, $-10 \le l \le +10$
reflections measured	18382
data reduction	
programs	IPDS-software, X-RED, X-SHAPE[39]
absorption correction	numerical
min/max transmission	0.3174/0.4045
unique reflections	1165
$R_{int}(F_o)$	0.0484
refinement	
programs	SHELXS-97, SHELXL-97[40]
parameters	36
observed reflections [$I_o > 2\sigma(I_o)$]	1075
$R(F_o)$[a] [$I_o > 2\sigma(I_o)$]; $R(F_o)$	0.0200; 0.0238
$R_w(F_o^2)$[b]	0.0409
goodness of fit	1.082
$\Delta\rho$ max/min [10^{-6} e pm^{-3}]	1.19/ – 1.14
twin law	1 0 0 0 1 0 0 0 – 1
fractional volume of major component	0.508(1)

[a] $R(F_o) = \Sigma||F_o| - |F_c||/\Sigma|F_o|$. [b] $R_w(F_o^2) = [\Sigma[w(F_o^2 - F_c^2)^2]/\Sigma[w(F_o^2)^2]]^{1/2}$; $w = 1/[\sigma^2(F_o^2) + (0.0226P)^2 + 0.2453P]$; $P = (F_o^2 + 2F_c^2)/3$.

Table 3. Atomic coordinates and equivalent displacement parameters, (U_{eq} [pm^2]) for Zr_5Te_6.

	site	x	y	z	U_{eq}
Te1	6*i*	0.89360(4)	0.10640(2)	0.28923(7)	57.0(9)
Te2	6*i*	0.55889(2)	0.44111(4)	0.20925(7)	56.3(9)
Te3	6*i*	0.77511(4)	0.22489(2)	0.75579(7)	81.9(13)
Zr1	1*a*	0	0	0	59(2)
Zr2	2*d*	1/3	2/3	0.5112(2)	82(2)
Zr3	6*g*	0.29940(5)	0	0	58.7(11)
Zr4	6*h*	0.63916(5)	0	1/2	104.7(12)

Table 4. Anisotropic displacement parameters [pm^2] for Zr_5Te_6.

	U_{11}	U_{22}	U_{33}	U_{23}	U_{13}	U_{12}
Te1	59(2)	50.9(12)	64(2)	– 7.4(7)	– 14.7(13)	29.7(8)
Te2	48.5(13)	56(2)	67(2)	– 14.8(14)	– 7.4(7)	28.1(8)
Te3	68(2)	59.4(14)	122(3)	21.8(8)	44(2)	33.9(9)
Zr1	73(3)	U_{11}	31(6)	0	0	36(2)
Zr2	102(3)	U_{11}	43(4)	0	0	51.0(13)
Zr3	61(2)	62(2)	54(3)	– 10(2)	– 4.8(11)	31.0(11)
Zr4	94(2)	U_{11}	50(3)	– 4.0(13)	4.0(13)	– 10(2)

Table 5. Selected interatomic distances [pm] for Zr_5Te_6.

Zr1–Te1 (×6)	297.53(5)	Zr4–Te2 (×2)	288.44(6)
Zr1–Zr3 (×6)	351.13(7)	Zr4–Te3 (×2)	292.63(4)
Zr2–Te3 (×3)	290.11(10)	Zr4–Te1 (×2)	299.31(7)
Zr2–Te2 (×3)	294.92(10)	Zr4–Zr4 (×1)	326.41(13)
Zr2–Zr4 (×6)	375.93(8)	Te1–Te1 (×2)	368.14(7)
Zr3–Te1 (×2)	283.50(6)	Te1–Te1 (×2)	374.35(5)
Zr3–Te3 (×2)	289.76(4)	Te1–Te3 (×2)	397.09(7)
Zr3–Te2 (×2)	302.56(6)	Te2–Te2 (×2)	379.20(8)
Zr3–Zr1 (×1)	351.13(7)	Te2–Te2 (×1)	380.50(7)
Zr3–Zr3 (×2)	351.13(7)	Te2–Te3 (×2)	388.59(7)
Zr3–Zr4 (×2)	360.76(5)	Te2–Te3 (×2)	397.66(5)
		Te3–Te3 (×2)	381.54(5)

Table 6. Parameters used for extended Hückel calculations.

	orbital	H_{ii} [eV]				ζ_1[a]	c_1[b]	ζ_2[a]	c_2[b]
		ZrTe	model **a**	model **b**	Zr_5Te_6				
Zr	5s	−7.674	−8.083	−8.150	−8.276	1.82			
	5p	−4.100	−4.438	−4.503	−4.639	1.78			
	4d	−7.336	−7.968	−8.069	−8.260	3.84	0.6213	1.505	0.5798
Te	5s		−21.20			2.51			
	5p		−12.00			2.16			

[a] Slater-type orbital exponents. [b] Coefficients used in double-ζ expansion.

magnetometer with a He cryostat. The data were corrected for diamagnetism of sample holders and atom cores.[41] Powdered samples of 50–200 mg of Zr_5Te_6 were loaded into the sample holder in an Ar-filled glovebox. Magnetization measurements for the normal state properties were carried out between 1.8 and 330 K in fields of 10 kG and 30 kG. The field dependence of the magnetization was measured at 5 K. For the superconducting-state properties, measurements with an external field of 20 to 100 G between 1.8 K and 10 K were carried out with field cooling (fc, Meissner effect) and zero-field cooling (zfc, diamagnetic shielding) of the samples. In order to determine the lower critical field (B_{c1}) a field scan ($-150\ \mathrm{G} \le B_{app} \le 150\ \mathrm{G}$) at 1.8 K was performed.

Electronic structure calculations: Band structure calculations on Zr_5Te_6, two hypothetical Zr_5Te_6 models **a** and **b**, and on a hypothetical stoichiometric ZrTe (NiAs type), were carried out within the tight-binding approximation at 80 k points by using the extended Hückel method.[42] For ZrTe (NiAs), reported lattice parameters[19] ($a = 396.2$, $c = 669.3$ pm) for a nominal composition of 52 atomic% Te were used. In hypothetical Zr_5Te_6 model **a**, NiAs-type ZrTe atomic coordinates and lattice parameters ($3a \times 3a \times 1c$) were used. For Zr_5Te_6 model **b**, the NiAs-type ZrTe atomic coordinates ($3a \times 3a \times 1c$) were retained, whereas the lattice parameters were relaxed to those of real Zr_5Te_6. In each case, the positions corresponding to the vacancies in Zr_5Te_6 were left empty. Valence-state ionization energies (H_{ii}) for Zr were obtained from charge-iterative calculations on the respective structures by using fixed valence-state ionization energies for Te. Other parameters have been cited elsewhere.[43] The parameters are listed in Table 6.

Acknowledgement

Financial support by the Deutsche Forschungsgemeinschaft and the Fonds der Chemischen Industrie is gratefully acknowledged. We would like to thank Dr. Stephan Debus for assistance with data collection on an IPDS diffractometer, Clemens Pietzonka and Rüdiger Penzel for magnetic and DSC measurements, respectively, and Dr. Thomas Degen, Philips, Almelo, NL, for powder XRD measurements performed with $Mo_{K\alpha}$ radiation.

[1] P. A. Maggard, J. D. Corbett, *J. Am. Chem. Soc.* **2000**, *122*, 838.
[2] R. L. Abdon, T. Hughbanks, *Angew. Chem.* **1994**, *106*, 2414; *Angew. Chem. Int. Ed. Engl.* **1994**, *33*, 2328.
[3] M. Conrad, F. Krumeich, B. Harbrecht, *Angew. Chem.* **1998**, *110*, 1454; *Angew. Chem. Int. Ed.* **1998**, *37*, 1383.
[4] H. Kleinke, W. Tremel, *Chem. Commun.* **1999**, 1175.
[5] M. Conrad, B. Harbrecht, *J. Alloys Compd.* **1992**, *187*, 181.
[6] a) F. K. McTaggart, A. D. Wadsley, *Aust. J. Chem.* **1958**, *11*, 445; b) H. Hahn, P. Ness, *Z. Anorg. Allg. Chem.* **1959**, *302*, 136.
[7] S. Furuseth, L. Brattås, A. Kjekshus, *Acta Chem. Scand.* **1973**, *27*, 2367.
[8] a) S. Furuseth, H. Fjellvåg, *Acta Chem. Scand.* **1991**, *45*, 694; b) C. Felser, E. W. Finckh, H. Kleinke, F. Rocker, W. Tremel, *J. Mater. Chem.* **1998**, *8*, 1787; c) K. Stöwe, F. R. Wagner, *J. Solid State Chem.* **1998**, *138*, 160.
[9] L. Brattås, A. Kjekshus, *Acta Chem. Scand.* **1973**, *27*, 1290.
[10] R. de Boer, E. H. P. Cordfunke, *J. Chem. Thermodyn.* **1999**, *31*, 105.
[11] C. Wang, C. Eylem, T. Hughbanks, *Inorg. Chem.* **1998**, *37*, 390.
[12] L. Brattås, A. Kjekshus, *Acta Chem. Scand.* **1971**, *25*, 2350.
[13] G. Örlygsson, B. Harbrecht, *Z. Naturforsch. Teil B* **1999**, *54*, 1125.
[14] G. Örlygsson, B. Harbrecht, unpublished results.
[15] G. Örlygsson, B. Harbrecht, *Z. Kristallogr. New Cryst. Struct.* **1999**, *214*, 5.
[16] R. de Boer, E. H. P. Cordfunke, P. van Vlaanderen, D. J. W. Ijdo, J. R. Plaisier, *J. Solid State Chem.* **1998**, *139*, 213.
[17] B. Harbrecht, R. Leersch, *J. Alloys Compd.* **1996**, *238*, 13.
[18] G. Örlygsson, B. Harbrecht, *Inorg. Chem.* **1999**, *38*, 3377.
[19] H. Sodeck, H. Mikler, K. L. Komarek, *Monatsh. Chem.* **1979**, *110*, 1.
[20] R. de Boer, E. H. P. Cordfunke, *J. Alloys Compd.* **1997**, *259*, 115.
[21] G. Örlygsson, B. Harbrecht, *Z. Kristallogr. Suppl. 16* **1999**, 52.
[22] M. Onoda, M. Saeki, *Acta Crystallogr. Sect. B* **1983**, *39*, 34.
[23] F. Jellinek, *Acta Crystallogr.* **1957**, *10*, 620.
[24] R. Brouwer, F. Jellinek, *Physica B* **1980**, *99*, 51.
[25] J. van Landuyt, G. A. Wiegers, S. Amelinckx, *Phys. Status Solidi A* **1978**, *46*, 479.
[26] J. Rouxel, *Chem. Eur. J.* **1996**, *2*, 1053.
[27] B. E. Brown, *Acta Crystallogr.* **1966**, *20*, 268.
[28] E. Canadell, M-H. Whangbo, *Inorg. Chem.* **1990**, *29*, 1398.
[29] M-H. Whangbo, E. Canadell, *J. Am. Chem. Soc.* **1992**, *114*, 9587.
[30] K. D. Bronsema, G. W. Bus, G. A. Wiegers, *J. Solid State Chem.* **1984**, *53*, 415.
[31] E. Canadell, S. Jobic, R. Brec, J. Rouxel, M-H. Whangbo, *J. Solid State Chem.* **1992**, *99*, 189.
[32] B. E. Brown, *Acta Crystallogr.* **1966**, *20*, 264.
[33] I. Kawada, M. Nakano-Onoda, M. Ishii, M. Saeki, M. Nakahira, *J. Solid State Chem.* **1975**, *15*, 246.
[34] A. Kallel, H. Boller, *J. Less-Common Met.* **1984**, *102*, 213.
[35] R. S. Mulliken, *J. Chem. Phys.* **1955**, *23*, 1833, 2343.
[36] C. P. Poole, Jr., *Handbook of Superconductivity*, Academic Press, San Diego, CA, **2000**, p. 449.
[37] R. D. Deslattes, A. Henins, *Phys. Rev. Lett.* **1976**, *36*, 898.
[38] V. Wagner, T. Degen, *DIFFRAKT (V 1.0)*, *A Program for Processing X-ray Powder Data*, University of Bonn (Germany), **1995**.
[39] a) *X-RED 1.07, Data reduction for STADI4 and IPDS*, STOE and Cie, Darmstadt (Germany), **1996**; b) *X-SHAPE 1.01*, *Crystal Optimisation for Numerical Absorption Correction*, STOE and Cie, Darmstadt (Germany), **1996**.
[40] a) G. M. Sheldrick, *SHELXS-97, Program for Crystal Structure Determination*, University of Göttingen (Germany), **1997**; b) G. M. Sheldrick, *SHELXL-97, Program for the Refinement of Crystal Structures*, University of Göttingen (Germany), **1997**.
[41] A. Weiss, H. Witte, *Magnetochemie*, VCH, Weinheim, **1973**, p. 95.
[42] a) R. J. Hoffmann, *J. Chem. Phys.* **1963**, *39*, 1397; b) M.-H. Whangbo, R. J. Hoffmann, *J. Am. Chem. Soc.* **1978**, *100*, 6093; c) M. Köckerling: *Program EHMACC*, adapted for use on PC by M. Köckerling, Gesamthochschule Duisburg (Germany), **1997**.
[43] E. Clementi, C. Roetti, *At. Data Nucl. Data Tables* **1974**, *14*, 177.

Received: March 24, 2000 [F2383]

  0947-6539/00/0622-4176 $ 17.50+.50/0